Mechanisms of Protein Fibril Formation: Nucleated Polymerization with Competing Off-Pathway Aggregation

Evan T. Powers* and David L. Powers†
*Department of Chemistry, The Scripps Research Institute, La Jolla, California; and †Department of Mathematics and Computer Science, Clarkson University, Potsdam, New York

ABSTRACT The formation of protein fibrils, and in particular amyloid fibrils, underlies many human diseases. Understanding fibril formation mechanisms is important for understanding disease pathology, but fibril formation kinetics can be complicated, making the relationship between experimental observables and specific mechanisms unclear. Here we examine one often-proposed fibril formation mechanism, nucleated polymerization with off-pathway aggregation. We use the characteristics of this mechanism to derive three tests that can be performed on experimental data to identify it. We also find that this mechanism has an especially striking feature: although increasing protein concentrations generally cause simple nucleated polymerizations to reach completion faster, they cause nucleated polymerizations with off-pathway aggregation to reach completion more slowly when the protein concentration becomes too high.

INTRODUCTION

The formation of fibrillar protein aggregates, often called amyloid fibrils, is a central feature of many human diseases (1), including the systemic amyloidoses (2), Alzheimer's disease (3), and Parkinson's disease (4) among others. The mechanism of protein fibril formation dictates the rate of protein fibril formation, the kinds of intermediates that exist during this process (which may be more toxic than the final products), and how long these intermediates persist. These factors, in turn, are likely to dictate disease onset and progression. In vitro studies of protein fibrillation mechanisms are therefore important for understanding diseases associated with protein fibril formation (5). Unfortunately, protein fibril formation mechanisms can be complicated, making it difficult to correlate experimental observations with specific mechanisms. Even the simple nucleated polymerization, in which a high-energy oligomer known as the nucleus acts as a bottleneck that limits the rate of fibril formation (6–9), can have unexpected features (9). This problem is aggravated when mechanisms include processes other than simple on-pathway fibril growth, such as formation of amorphous (i.e., nonfibrillar) aggregates. Such complications are quite common in experimental studies of protein fibril formation (10–24). Nonfibrillar aggregates could play several roles in fibril formation mechanisms: they could be necessary for fibril formation (obligate); they could be capable of converting to fibrils but not necessary for fibril formation (on-pathway); or they could be incapable of converting directly to fibrils (off-pathway). Distinguishing among these possibilities can be difficult, but is critical for understanding fibril formation kinetics. In this report, we propose tests that can be applied to experimental data to identify nucleated polymerizations with competing off-pathway aggregation. We use analytical approximations and numerical solutions to the rate equations to show that, under some conditions, nucleated polymerizations with off-pathway aggregation have simple kinetics and we derive equations that can be fit to experimental reaction progress data. Furthermore, we show that off-pathway aggregates retard fibril formation and in addition can cause the fibril formation rate to have an inverted concentration dependence; that is, fibril formation can become slower as the protein concentration increases.

MATERIALS AND METHODS

Numerical integration of differential equations and other calculations were performed on a personal computer with dual AMD Athlon 2200 MP processors using Mathematica 5.2 (Wolfram Research, Champaign, IL) for Windows XP.

RESULTS

Model

Fig. 1 is an illustration of our model for a nucleated polymerization with competing off-pathway aggregation. As indicated in Fig. 1, the monomer is denoted X_1. On-pathway species are denoted Y_j ($j \geq 2$). The nucleus consists of n monomers and is denoted Y_n; on-pathway species smaller than the nucleus are called oligomers, and those larger than the nucleus are called fibrils. Off-pathway species are denoted Z_j ($j \geq 2$) and are called aggregates. This model contains the following assumptions, most of which are common in models of protein fibril formation and aggregation (7–9,25–27). 1), We assume that the sizes of both on-pathway fibrils and off-pathway aggregates change only by monomer association or dissociation (Roberts (28) and Andrews and Roberts (8) have recently characterized models that include association by larger species). 2), We assume

Submitted July 10, 2007, and accepted for publication September 7, 2007.
Address reprint requests to Evan T. Powers, E-mail: epowers@scripps.edu.
Editor: Ruth Nussinov.

0006-3495/08/01/379/13 $2.00
doi: 10.1529/biophysj.107.117168

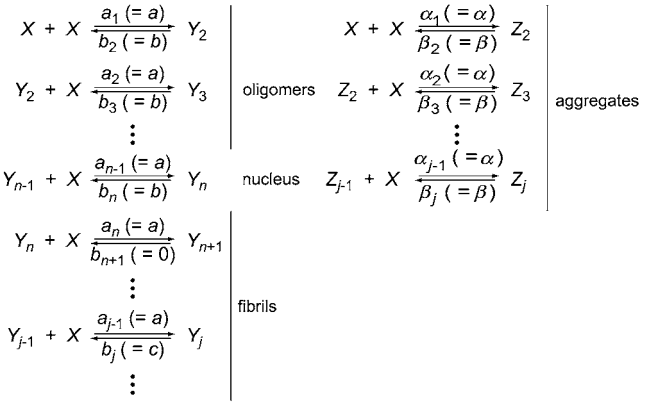

FIGURE 1 The nucleated polymerization mechanism of fibril formation with off-pathway aggregation. Both on-pathway (denoted Y_j) and off-pathway species (denoted Z_j) are assumed to grow only by monomer addition. The on-pathway species with n subunits (Y_n) is known as the nucleus; on-pathway species with fewer than n subunits are referred to as oligomers, whereas those with more than n subunits are referred to as fibrils. All off-pathway species are referred to as aggregates. The letters above and below the arrows represent rate constants for the corresponding reactions. The rate constants in parentheses result from the assumptions in the text.

that addition of a monomer to the nucleus to form a fibril is irreversible ($b_{n+1} = 0$). This assumption enables us to treat all of the fibrils together, where the fibril number concentration is denoted $[F^{(0)}]$ ($[F^{(0)}] = \sum_{j=n+1}^{\infty}[Y_j]$) and the amount of monomer incorporated into fibrils, or the fibril amount concentration, is denoted $[F^{(1)}]$ ($[F^{(1)}] = \sum_{j=n+1}^{\infty} j[Y_j]$). The quantities $[F^{(0)}]$ and $[F^{(1)}]$ are the 0th and 1st moments of the fibril size distribution (29). 3), We assume that on-pathway association rate constants are independent of size ($a_1 = a_2 = a_3 = \ldots = a$). We assume the same for off-pathway association rate constants ($\alpha_1 = \alpha_2 = \alpha_3 = \ldots = \alpha$), but we expect α to be larger than a: because the off-pathway aggregates are amorphous, the orientational requirements for monomer addition should be more relaxed than for the more structured fibrils (30–32). (Association rate constants cannot be truly size independent, but Hill has shown that monomer-monomer and monomer-large fibril association rate constants should be different by a factor of no more than two (27).) 4), We assume that on-pathway dissociation rate constants are the same for all oligomers ($b_2 = b_3 = \ldots b_n = b$), but they decrease sharply after the nucleus (reflecting the greater stability of fibrils) and are constant thereafter ($b_{n+2} = b_{n+3} = \ldots = c$, $c \ll b$). We assume that the off-pathway dissociation rate constants are completely size independent ($\beta_2 = \beta_3 = \ldots = \beta$) because, unlike the on-pathway species, amorphous aggregates are unlikely to have structural features that change at a critical size. 5), We assume that off-pathway aggregates are less stable than fibrils but more stable than oligomers. We make this assumption because if off-pathway aggregates were more stable than fibrils, their higher association rate constants would preclude fibril formation, whereas if they were less stable than oligomers, off-pathway aggregation would not happen. 6), Finally, we assume that fibrils do not associate to form fibril clusters (which are sometimes observed in fibril formation reactions), or, equivalently, we assume that if such fibril association happens, it does not affect the elongation kinetics of individual fibrils in the clusters.

The relative stabilities of the species in the mechanism in Fig. 1 can be characterized by their monomer dissociation constants. For a fibril, this dissociation constant is $K_c = c/a$. This quantity is also known as the ''critical concentration'' for fibril formation because fibril formation is negligible if the total protein concentration ($[X]_{tot}$) is $<K_c$ (7,24,25). The monomer dissociation constant from an oligomer is $K_s = b/a$. We have previously named this quantity the ''supercritical concentration'' because the monomer, not the nucleus, becomes the highest energy species on the fibril formation pathway when $[X]_{tot} > K_s$ (9). Finally, the monomer dissociation constant from an off-pathway aggregate is $K_A = \beta/\alpha$. Given the fifth assumption made in the preceding paragraph, the equilibrium constants for monomer dissociation increase in the order $K_c < K_A < K_s$ (also note that $\beta \gg c$ because $K_c < K_A$ and $\alpha > a$).

The third and fourth assumptions made above guarantee that the size of the on-pathway nucleus will be independent of concentration (as long as $[X]_{tot} < K_s$) (6,9). Such constant nucleus size models are appropriate for fibrils with structures in which there is a sudden change in the number of contacts made by added subunits once a critical size is reached; for example, at the closing of the first loop in a helical fibril (6,7,9,27,33). The nucleus is then the species one subunit smaller than this critical size. However, for reasons given by Ferrone (6), this model breaks down even for helical polymers if the nucleus is too large. Thus, in this work we treat only cases with $n \leq 5$. The third and fourth assumptions also guarantee that off-pathway aggregation is not nucleated (i.e., it is a downhill polymerization when $[X]_{tot} > K_A$), since neither the association nor the dissociation rate constants for this process change with aggregate size.

A final consequence of our assumptions is that, because off-pathway aggregation is not nucleated and because monomer association and dissociation are both faster off-pathway than on-pathway ($\alpha > a$ and $\beta \gg c$), off-pathway aggregation comes to equilibrium almost before fibril formation begins. In fact, we show in the Supplementary Material that the off-pathway aggregate size distribution approaches equilibrium with an effective half-life ($t_{1/2}$) of

$$t_{1/2} = \frac{\ln 2}{\beta\left(1 - \sqrt{1 + \frac{K_A - \sqrt{4K_A[X]_{tot} + K_A^2}}{2[X]_{tot}}}\right)^2}. \quad (1)$$

This timescale is substantially shorter than that of fibril formation for all cases examined herein. We can therefore treat the monomer as though it is in continuous preequili-

brium with off-pathway aggregates during fibril formation; that is aggregates instantaneously compensate for any changes in monomer concentration such that the monomer-aggregate preequilibrium is maintained (we use the term ''preequilibrium'' here rather than ''equilibrium'' because true equilibrium is not reached until fibril formation is complete). In this sense, the aggregates could be said to buffer the monomer concentration (see below). This result makes it convenient to combine to the monomer and the off-pathway aggregates into the quantity $[A]$, the amount concentration of monomer plus aggregates: $[A] = [X_1] + \sum_{j=2}^{\infty} j[Z_j]$. The concentrations of the Z_j at equilibrium are $[Z_j] = [X_1]^j/K_A^{j-1}$, so the expression for $[A]$ can be simplified:

$$[A] = \sum_{j=1}^{\infty} j[X_1]^j/K_A^{j-1} = \frac{[X_1]K_A^2}{(K_A - [X_1])^2}. \quad (2)$$

Solving Eq. 2 for $[X_1]$ gives the concentration of monomer in preequilibrium with off-pathway aggregates, which we will denote $[X_1]_e$:

$$[X_1]_e = K_A\left(1 + \frac{K_A - \sqrt{4K_A[A] + K_A^2}}{2[A]}\right). \quad (3)$$

Fig. 2 is a plot of $[X_1]_e/K_A$ as a function of $[A]/K_A$, showing that $[X_1]_e/K_A$ asymptotically approaches 1 as $[A]/K_A$ becomes large (i.e., $[X_1]_e$ approaches K_A when $[A] \gg K_A$).

The rate equations for the mechanism shown in Fig. 1 are presented in the Supplementary Material. Given the assumptions made above, however, these rate equations can be simplified. Because monomer and off-pathway aggregates are in preequilibrium, the rate equations for $[X_1]$ and $[Z_j]$ ($j \geq 2$) can be replaced by the single rate equation for $[A]$. Moreover, because the monomer concentration is always below the supercritical concentration ($[X_1]_e \leq K_A < K_s$), the simplifications made for classical nucleated polymerizations (6–8) can be made here: the rate equations for oligomers can be ignored because their concentrations are negligible, and, like the off-pathway aggregates, the nucleus is in preequilibrium with monomer ($[Y_n] = [X_1]_e^n/K_s^{n-1}$). Applying these simplifications to the rate equations in the Supplementary Material yields the following (see the Supplementary Material for more details):

$$\frac{d[A]}{dt} = -(n+1)a[X_1]_e[Y_n] - a[X_1]_e[F^{(0)}] + c[F^{(0)}]$$
$$= \frac{-(n+1)a[X_1]_e^{n+1}}{K_s^{n-1}} - a[X_1]_e[F^{(0)}] + c[F^{(0)}] \quad (4)$$

$$\frac{d[F^{(0)}]}{dt} = a[X_1]_e[Y_n] = \frac{a[X_1]_e^{n+1}}{K_s^{n-1}} \quad (5)$$

$$\frac{d[F^{(1)}]}{dt} = (n+1)a[X_1]_e[Y_n] + a[X_1]_e[F^{(0)}] - c[F^{(0)}]$$
$$= \frac{(n+1)a[X_1]_e^{n+1}}{K_s^{n-1}} + a[X_1]_e[F^{(0)}] - c[F^{(0)}] \quad (6)$$

$$[X]_{tot} = [A] + [F^{(1)}] \quad (7)$$

$$[A]_{t=0} = [X]_{tot}, \quad [F^{(0)}]_{t=0} = 0, \quad [F^{(1)}]_{t=0} = 0, \quad (8)$$

where $[X_1]_e$ is given by Eq. 3. In the above set of equations, Eq. 4 is the rate equation for the combined amount concentration of monomer and off-pathway aggregates. It comprises three terms: the first accounts for protein passing from the monomer/off-pathway aggregate state to the fibril state through the formation of new fibrils, which consumes $n + 1$ monomers; the second accounts for protein passing from the monomer/off-pathway aggregate state to the fibril state through monomer addition to already existing fibrils; the third accounts for protein passing from the fibril state to the monomer/off-pathway aggregate state through monomer dissociation from fibrils. Equation 5 is the rate equation for the fibril number concentration, $[F^{(0)}]$. It consists of only one positive term (reflecting the nucleation of new fibrils) because we have assumed that fibril formation is irreversible (see assumption 2 above). Equation 6 is the rate equation for the fibril amount concentration, $[F^{(1)}]$ (i.e., the amount of protein incorporated into fibrils). It is the negative of Eq. 4 because, as mentioned above, we have ignored oligomers, leaving monomers/off pathway aggregates and fibrils as the only remaining states. Any protein that leaves one of these states has to enter the other. This reasoning also explains Eq. 7, the mass balance equation, which states that the total protein concentration is the sum of the monomer/off-pathway aggregate amount concentration and the fibril amount concentration. Finally, in Eq. 8 are the initial conditions.

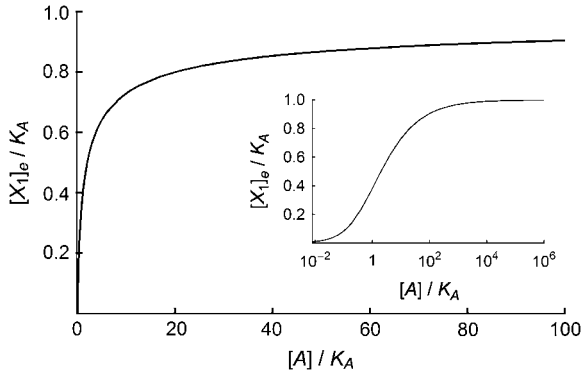

FIGURE 2 The equilibrium concentration of monomer, $[X_1]_e$, in the presence of a given amount of off-pathway aggregate, $[A]$. Both monomer and off-pathway aggregate are measured relative to K_A, the equilibrium constant for monomer dissociation from an off-pathway aggregate. (*Inset*) Same as above, but shown on a log scale to illustrate the asymptotic approach of $[X_1]_e/K_A$ to 1 as $[A]$ increases.

Equations 4–8 do not have a steady-state solution (because $d[F^{(0)}]/dt$ is always positive), but steady state is most closely approached when $[X_1]_e = c/a = K_c$ (9). Substituting this into Eq. 2 gives the near steady-state amount concentration of monomer plus off-pathway aggregates, $[A]_{ss} = (K_c K_A^2)/(K_A - K_c)^2$, which can be substituted into Eq. 7 to give the

near steady-state amount concentration of fibrils, $[F^{(1)}]_{ss} = ([X]_{tot} - K_c K_A^2)/(K_A - K_c)^2$. If $K_A \gg K_c$, this simplifies to $[F^{(1)}]_{ss} = [X]_{tot} - K_c$, which implies that the concentration of off-pathway aggregates is negligible at steady state. Equations 4–8 are valid until the near steady-state point is reached, but because $[F^{(0)}]$ continues to increase beyond this point (whereas the actual fibril number concentration should decrease), the approximation breaks down at long times (7).

The effect of off-pathway aggregation on fibril formation kinetics: a test case and analytical approximations

The solid curves in Fig. 3 are plots of the numerical solutions to the rate equations for our model for a test case in which $[X]_{tot}$ is varied from 1 μM to 10 mM and the other parameters are fixed: $n = 4$, $K_c = 100$ nM, $K_s = 100$ μM, $a = 10^6$ $M^{-1}s^{-1}$ ($b = 10^2$ s^{-1}, $c = 10^{-1}$ s^{-1}), $K_A = 1$ μM, $\alpha = 10^7$ $M^{-1}s^{-1}$ ($\beta = 10$ s^{-1}). The progress of the reaction is shown in terms of the fraction of protein that has been converted to fibrils ($[F^{(1)}]/[F^{(1)}]_{ss}$), which can be determined experimentally by dye binding assays discussed in more detail below. The more complete set of rate equations in the Supplementary Material was used to obtain the numerical solutions plotted in Fig. 3 instead of Eqs. 4–8. This was done to ensure that our assumption that the monomer and off-pathway aggregates are immediately and continuously in preequilibrium does not unduly bias our examination of this mechanism. Fig. 3 shows that the time courses of fibril formation are roughly sigmoidal at low $[X]_{tot}$ ($[X]_{tot} \leq 10$ μM), with $[F^{(1)}]/[F^{(1)}]_{ss}$ increasing slowly at first, then more rapidly as the reaction progresses, and slowly again as fibril formation approaches completion. The appearance of the time courses changes as $[X]_{tot}$ increases: at high $[X]_{tot}$ ($[X]_{tot} \geq 100$ μM) the fibril formation rate increases continually until the reaction is almost complete, at which point it abruptly drops to ~0. In addition, Fig. 3 shows that the concentration dependence of the fibril formation rate is unusual. Fig. 3 *F* is a log-log plot of the t_{50} for fibril formation (the time required for fibril formation to reach 50% completion) versus $[X]_{tot}$ showing that t_{50} initially decreases as $[X]_{tot}$ increases (as expected for a fibril formation reaction (7,9,25,26)), but t_{50} reaches a minimum at around 10 μM and then begins to increase as $[X]_{tot}$ increases; that is, the approach to completion becomes slower as the protein concentration increases. This ''inverted'' dependence of t_{50} on $[X]_{tot}$ has been observed experimentally in the aggregation of immunoglobulin light chain (22,23) and the prion protein (11).

These observations can be understood by noting that, as several groups have observed previously (18,19,34,35), off-pathway aggregates serve as a reservoir of protein from which the monomer draws as it is consumed to form fibrils. The off-pathway aggregates buffer the monomer concentration, which therefore changes slowly as fibrils form. Because of this behavior, it is instructive to solve Eqs. 4–8 as though $[X_1]_e$ were constant and equal to its initial value, given by substituting $[A] = [X]_{tot}$ into Eq. 3:

$$[X_1]_{e,t=0} = K_A\left(1 + \frac{K_A - \sqrt{4K_A[X]_{tot} + K_A^2}}{2[X]_{tot}}\right). \quad (9)$$

Equations 4–8 are then easily solved:

$$[A] = [X]_{tot} - \frac{[X_1]_{e,t=0}^{n+1}}{K_s^{n-1}}\left[(n+1)at + \frac{([X_1]_{e,t=0} - K_c)}{2}a^2t^2\right] \quad (10)$$

$$[F^{(0)}] = \frac{[X_1]_{e,t=0}^{n+1}}{K_s^{n-1}}at \quad (11)$$

$$[F^{(1)}] = \frac{[X_1]_{e,t=0}^{n+1}}{K_s^{n-1}}\left[(n+1)at + \frac{([X_1]_{e,t=0} - K_c)}{2}a^2t^2\right]. \quad (12)$$

Equations 10–12 show that, as long as $[X_1]_e \sim [X_1]_{e,t=0}$, $[F^{(0)}]$ increases linearly with time, $[F^{(1)}]$ increases as t^2, and $[A]$ decreases as t^2. Inspecting Eqs. 10–12 makes it clear that treating $[X_1]_e$ as a constant is an approximation that cannot be valid over the entire fibril formation time course, since the expressions for $[F^{(0)}]$ and $[F^{(1)}]$ increase without bound as t increases. Ferrone has obtained similar results using a constant monomer concentration approximation for simple nucleated polymerizations, and has shown that this approximation is only valid for the first 10–20% of the time course, after which the monomer concentration begins to depart appreciably from its initial value (25). Fortunately, when the monomer concentration is buffered by an off-pathway aggregation, $[X_1]_e$ remains close to its initial value for larger and larger portions of the fibril formation time course as $[X]_{tot}$ increases. This observation is illustrated by the long-dashed curves in Fig. 3, which are plots of $[F^{(1)}]/[F^{(1)}]_{ss}$ made by using Eq. 12. At low $[X]_{tot}$ ($[X]_{tot} = 1$ μM, Fig. 3 *A*), the approximation is good only until $[F^{(1)}]/[F^{(1)}]_{ss} \sim 0.1$. The inset in Fig. 3 *A* shows that $[X_1]_e$ deviates substantially from $[X_1]_{e,t=0}$ beyond this point. As $[X]_{tot}$ increases to moderate values ($[X]_{tot} = 10$–100 μM, Fig. 3, *B* and *C*), $[X_1]_e$ remains closer to $[X_1]_{e,t=0}$ over more of the fibril formation time course, so Eq. 12 is valid for longer. However, Fig. 3, *D* and *E*, show that Eq. 12 is not a good approximation to the actual time courses as $[X]_{tot}$ increases beyond 100 μM, despite $[X_1]_e$ being very close to $[X_1]_{e,t=0}$ throughout fibril formation.

The deviation of Eq. 12 from the numerical solutions at high concentration can be explained by noting that the deviations begin when $[X]_{tot}$ exceeds the supercritical concentration ($K_s = 100$ μM). At such high protein concentrations, on-pathway oligomers become stable. The fibril formation pathway behaves initially like an irreversible downhill polymerization instead of a nucleated polymerization (9), and protein floods into both the fibril formation and the aggregation pathways. Instead of coming to a preequilibrium, monomer partitions between the pathways according to the ratio

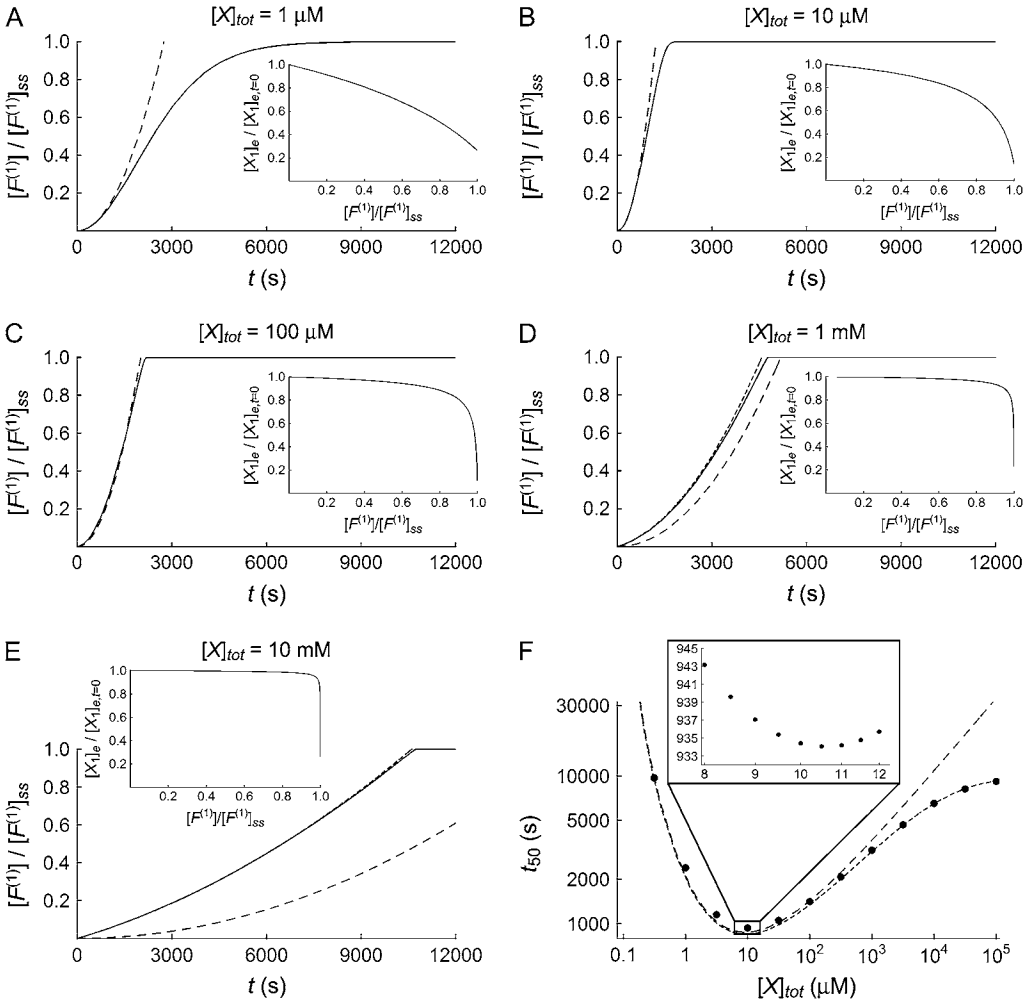

FIGURE 3 (*A–E*) Plots of the extent of completion versus time for our test case at (*A*) $[X]_{tot} = 1\ \mu M$, (*B*) $[X]_{tot} = 10\ \mu M$, (*C*) $[X]_{tot} = 100\ \mu M$, (*D*) $[X]_{tot} = 1$ mM, and (*E*) $[X]_{tot} = 10$ mM. The extent of completion is defined as the amount concentration of fibrils ($[F^{(1)}]$) relative to the near steady-state amount concentration of fibrils ($[F^{(1)}]_{ss}$). Solid curves represent the time courses obtained from the numerical solutions to the rate equations. Long-dashed curves represent time courses obtained from Eq. 12. Short-dashed curves (*D* and *E* only) represent time courses obtained from Eq. 15 using values of $[F^{(0)}]_0$ calculated as described in the Supplementary Material. (*Insets*) Plots of the monomer concentration ($[X_1]_e$) relative to initial monomer concentration ($[X_1]_{e,t=0}$) as a function of the extent of completion. (*F*) A plot of t_{50} vs. $[X]_{tot}$ on a log-log scale. Points represent t_{50} values calculated from the numerical solutions of the rate equations. The long-dashed curve represents t_{50} values calculated from Eq. 16. The short-dashed curve represents t_{50} values calculated from Eq. 18. (*Inset*) An expansion of the region around $[X]_{tot} = 10\ \mu M$ showing that the minimum t_{50} value occurs at $[X]_{tot} = 10.5\ \mu M$.

α/a; that is, their relative association rates control the amounts of off-pathway and on-pathway species that form, not their relative stabilities (we have observed similar effects in tetramerization by competing pathways (36)). The monomer concentration decreases as the reaction proceeds, and when it is low enough the now-unstable on-pathway oligomers dissociate in favor of off-pathway aggregates. Preequilibrium is then established between the pathways. However, any fibrils that formed during the initial rush of protein into the fibril formation pathway are stable and persist even after the monomer reaches equilibrium with the off-pathway aggregates. Such fibrils act as seeds for fibril formation, causing the fibril formation reaction to progress faster than would be expected based on Eqs. 10–12. This behavior can be accounted for by changing the initial condition for $[F^{(0)}]$ from $[F^{(0)}]_{t=0} = 0$ to $[F^{(0)}]_{t=0} = [F^{(0)}]_0$ where $[F^{(0)}]_0$ is a constant. Solving Eqs. 4–8 with $[F^{(0)}]_{t=0} = [F^{(0)}]_0$ and retaining the approximation that $[X_1]_e = [X_1]_{e,t=0} =$ constant gives the following results:

$$[A] = [X]_{tot} - [F^{(0)}]_0([X_1]_{e,t=0} - K_c)at - \frac{[X_1]_{e,t=0}^{n+1}}{K_s^{n-1}}\left[(n+1)at + \frac{([X_1]_{e,t=0} - K_c)}{2}a^2t^2\right] \quad (13)$$

$$[F^{(0)}] = [F^{(0)}]_0 + \frac{[X_1]_{e,t=0}^{n+1}}{K_s^{n-1}}at \quad (14)$$

$$[F^{(1)}] = [F^{(0)}]_0([X_1]_{e,t=0} - K_c)at + \frac{[X_1]_{e,t=0}^{n+1}}{K_s^{n-1}}\left[(n+1)at + \frac{([X_1]_{e,t=0} - K_c)}{2}a^2t^2\right]. \quad (15)$$

Equations 13–15 contain extra terms that are directly proportional to $[F^{(0)}]_0$. The extra terms are independent of t for $[F^{(0)}]$ and linear in t for $[A]$ and $[F^{(1)}]$. The influence of the extra linear term in the expression for $[F^{(1)}]$ is apparent in Fig. 3, *D* and *E*, where the numerically solved fibril formation time courses are less curved than in Fig. 3, *A–C*. The value of $[F^{(0)}]_0$ can be estimated from first principles, as demonstrated in the Supplementary Material. This estimate was used in Eq. 15 to draw the short-dashed curves in Fig. 3, *D* and *E*. These plots show that accounting for fibrils formed during the initial wave of fibril formation at high total protein concentration ($[X]_{tot} > K_s$) greatly improves the approximation to the numerical solutions. The expression for $[F^{(0)}]_0$ is cumbersome and is not reproduced here (see Supplementary Material), but we note that $[F^{(0)}]_0$ is directly proportional to $[X]_{tot}$, and it increases as α/a decreases (that is, as the rate of on-pathway fibril formation increases relative to off-pathway aggregation) and as n decreases (because small nuclei make fibril formation easier).

Equations 12 and 15 (the approximate solutions for $[F^{(1)}]$) can be used to explain the unusual dependence of t_{50} on $[X]_{tot}$ alluded to above and illustrated by Fig. 3 *F*. A simple estimate of t_{50} can be obtained by solving Eq. 12 for t when $[F^{(1)}] = [X]_{tot}/2$, the approximate halfway point for fibril formation:

$$t_{50} = \frac{1}{a}\sqrt{\frac{K_s^{n-1}[X]_{tot}}{[X_1]_{e,t=0}^{n+1}([X_1]_{e,t=0} - K_c)}}. \quad (16)$$

We have ignored the linear term in Eq. 12 to obtain this equation since it becomes negligible when $t \gg 2\,(n+1)\,a^{-1}([X_1]_{e,t=0} - K_c)^{-1}$, which usually happens early in the fibril formation time course (after ~10 s in our test case). Equation 16 is plotted in Fig. 3 *F* as the long-dashed curve. Since Eq. 16 was derived from Eq. 12, all of the limitations of Eq. 12 apply to Eq. 16 as well. Equation 16 is therefore less accurate at low and high values of $[X]_{tot}$ than at moderate values of $[X]_{tot}$. Nevertheless, it reproduces the most striking feature of the dependence of t_{50} on $[X]_{tot}$: the change from a negative to a positive slope in the plot of t_{50} vs. $[X]_{tot}$ as $[X]_{tot}$ increases. This change in slope indicates that the fibril formation rate (relative to the total protein concentration) begins to slow down as $[X]_{tot}$ increases beyond a critical value. Mathematically, this behavior can be explained by the dependence of $[X_1]_{e,t=0}$ on $[X]_{tot}$. The value of $[X_1]_{e,t=0}$ initially increases fairly rapidly as $[X]_{tot}$ increases (the initial slope of a plot of $[X_1]_{e,t=0}$ vs. $[X]_{tot}$ is 1; see Fig. 2). Consequently, the denominator of Eq. 16 increases faster than the numerator (especially since the denominator depends on the $n + 2$ power of $[X_1]_{e,t=0}$) and t_{50} decreases as $[X]_{tot}$ increases. However, the dependence of $[X_1]_{e,t=0}$ on $[X]_{tot}$ soon weakens and $[X_1]_{e,t=0}$ eventually becomes almost constant, approaching K_A asymptotically. The denominator of Eq. 16 also becomes nearly constant, but the numerator continues to increase, so t_{50} eventually begins to increase as $[X]_{tot}$ increases. It can be shown (see Supplementary Material) that the change in the sign of the slope of the t_{50} vs. $[X]_{tot}$ plot happens when

$$[X]_{tot} = \frac{K_A(n^2 + 4n + 3)}{4}. \quad (17)$$

In our test case, $n = 4$ and $K_A = 1\ \mu M$, so according to Eq. 17 the sign change in the slope should occur at 8.8 μM. The inset to Fig. 3 *F* shows that the sign change in the slope in fact occurs at around 10.5 μM according to the numerical solutions, matching the result from Eq. 17 to within ~0.1 log units. Physically, the explanation given above for the change in slope in plots of t_{50} vs. $[X]_{tot}$ translates to the following. Off-pathway aggregation limits the monomer concentration to be $< K_A$, no matter how high the total protein concentration is, and therefore limits the rate of fibril formation as well. However, the amount of protein that must be converted to fibrils is not limited. The time required for fibril formation to reach 50% completion thus increases as $[X]_{tot}$ increases when $[X]_{tot}$ is very high.

After the plot of t_{50} vs. $[X]_{tot}$ changes slope, it increases rapidly at first, then more slowly. This behavior is not captured by Eq. 16, inspection of which suggests that t_{50} should increase with $[X]_{tot}^{1/2}$ (the slope of the log-log plot should be +1/2). Better estimates of t_{50} at high protein concentrations can be obtained by solving Eq. 15 (instead of Eq. 12) for t when $[F^{(1)}] = [X]_{tot}/2$. This yields

$$t_{50} = \frac{1}{a\left[\frac{[F^{(0)}]_0([X_1]_{e,t=0} - K_c)}{[X]_{tot}} + \sqrt{\left(\frac{[F^{(0)}]_0([X_1]_{e,t=0} - K_c)}{[X]_{tot}}\right)^2 + \frac{[X_1]_{e,t=0}^{n+1}([X_1]_{e,t=0} - K_c)}{[X]_{tot}K_s^{n-1}}}\right]}. \quad (18)$$

(We have again ignored the term $[X_1]_{e,t=0}^{n+1}(n+1)at/K_s^{n-1}$ to obtain this equation. Also note that Eq. 18 is identical to Eq. 17 when $[F^{(0)}]_0 = 0$.) Equation 18 is plotted in Fig. 3 *F* as the short-dashed curve. This plot shows that it is a substantially better approximation to the t_{50} values at high

$[X]_{tot}$ (>100 μM) than Eq. 17. It can therefore be used to understand the dependence of t_{50} on $[X]_{tot}$ at high $[X]_{tot}$. At first glance, it appears that all of the terms in the denominator of Eq. 18 are functions of $[X]_{tot}$. However, as mentioned above, $[F^{(0)}]_0$ is directly proportional to $[X]_{tot}$, so it can be written $[F^{(0)}]_0 = f_0[X]_{tot}$ where f_0 is a proportionality constant. Furthermore, $[X_1]_{e,t=0}$ depends weakly on $[X]_{tot}$ when $[X]_{tot}$ is large; $[X_1]_{e,t=0}$ only changes from 0.90 to 0.99 μM as $[X]_{tot}$ changes from 100 μM to 100 mM, so $[X_1]_{e,t=0}$ can be replaced by K_A in this concentration range (recall that $K_A = 1$ μM). These two observations allow us to rewrite Eq. 18 in a form that illustrates more clearly the dependence of t_{50} on $[X]_{tot}$ at high $[X]_{tot}$:

$$t_{50} = \frac{1}{a\left[f_0(K_A - K_c) + \sqrt{(f_0(K_A - K_c))^2 + K_A^{n+1}(K_A - K_c)[X]_{tot}^{-1}K_s^{-n+1}}\right]}. \quad (19)$$

Two extremes are of interest here. If f_0 is small and $[X]_{tot}$ is not too large (formally, if the inequality $[X]_{tot} \ll K_A^{n+1}/\left(K_s^{n-1}(K_A - K_c)f_0^2\right)$ holds), then the first two terms in the denominator can be neglected, Eq. 19 reduces to Eq. 16, and t_{50} is proportional to $[X]_{tot}^{1/2}$ so that the slope of a log-log plot of t_{50} vs. $[X]_{tot}$ would be +1/2. The square-root dependence of t_{50} on $[X]_{tot}$ can be explained by the dependence of $[F^{(1)}]$ on t^2, which in turn is a consequence of the constant monomer concentration (and therefore the constant rate of fibril nucleation). On the other hand, if f_0 and $[X]_{tot}$ are both large enough (if the inequality $[X]_{tot} \gg K_A^{n+1}/(K_s^{n-1}(K_A - K_c)f_0^2)$ holds), then the last term in the denominator can be neglected and Eq. 19 reduces to

$$t_{50} = \frac{1}{2af_0(K_A - K_c)}. \quad (20)$$

The value of t_{50} is independent of $[X]_{tot}$ in this regime, and a log-log plot of t_{50} vs. $[X]_{tot}$ would have a slope of 0. This independence can be explained by noting that at such high protein concentrations, the amount of fibrils formed during the irreversible polymerization stage of the fibril formation time course is much larger than the amount of fibrils nucleated during preequilibrium. Consequently, only the term $[F^{(0)}]_0([X_1]_{e,t=0} - K_c)at = f_0[X]_{tot}([X_1]_{e,t=0} - K_c)at$ in Eq. 15 is significant, so $[F^{(1)}]$ depends linearly on t with a slope that is proportional to $[X]_{tot}$. Thus, the time it takes $[F^{(1)}]$ to reach $0.5[X]_{tot}$ has to be independent of $[X]_{tot}$. To summarize our analysis of the dependence of t_{50} on $[X]_{tot}$: t_{50} initially decreases as $[X]_{tot}$ increases, as expected for fibril formation reactions, but it reaches a minimum at a concentration given approximately by Eq. 17 and then increases. Beyond this point, a log-log plot of t_{50} vs. $[X]_{tot}$ should have a positive slope of at most +1/2, which should decrease gradually toward 0 as $[X]_{tot}$ increases. This behavior is observed over a wide range of parameter values, although it changes subtly when K_s/K_A becomes larger than ~1000 (see Supplementary Material).

Connection to experiment: experimentally measurable quantities

Before discussing how the results in the preceding section can be used to identify a nucleated polymerization with off-pathway aggregation, we will discuss the techniques available to measure the quantities that are accessible from the analysis above. The time-dependent value of $[F^{(1)}]/[F^{(1)}]_{ss}$, which corresponds to the fraction completion of a fibril formation reaction and is accessible from Eqs. 12 or 15, can be determined experimentally using the binding of certain dyes to amyloid fibrils (e.g., thioflavin T (37,38)). For proteins that do not precipitate during fibril formation, fraction completion also can be measured by spectroscopic techniques like circular dichroism (CD), or any other technique that responds linearly to the concentration of amyloid. Whether dye binding, CD spectroscopy, or some other technique is used, the fraction completion, which we will denote χ, is given by

$$\chi = \frac{(S_t - S_i)}{(S_f - S_i)} = \frac{[F^{(1)}]}{[F^{(1)}]_{ss}}, \quad (21)$$

where S_t is the signal measured by the chosen technique at time t, S_i is the signal at $t = 0$, and S_f is the signal at the end of the fibril formation reaction. The t_{50} of a fibril formation reaction, which is accessible from Eqs. 16 or 18, can be determined experimentally by identifying the time at which χ, measured as described above, is equal to 0.5. Finally, an expression for the time dependence of the intensity of scattered light from a nucleated polymerization with an off-pathway aggregation can be derived using the assumption of preequilibrium between monomers and amorphous aggregates and Eqs. 13 or 17 (see below). Other quantities relevant to fibril formation reactions, like the monomer concentration (39–41) or the fibril size distribution (42,43), can also be measured. However, our analysis did not yield simple expressions for the time dependence of either of these quantities, so we will focus on using χ, t_{50} values, and light scattering for identifying fibril formation mechanisms.

Connection to experiment: the use of χ vs. t data

Equation 15 shows that $\chi = [F^{(1)}]/[F^{(1)}]_{ss}$ should have a quadratic time dependence as long as $[X_1]_e$ is close to its initial

value. It should therefore be possible to fit at least part of a plot of χ vs. t to the equation

$$\chi = C_1 t + C_2 t^2. \tag{22}$$

Of course, this is also true for nucleated polymerizations (25,44), so a good fit of Eq. 22 to the early portion of an experimental fibril formation time course alone cannot be used to identify a nucleated polymerization with an off-pathway aggregation. A stronger test for the existence of an off-pathway aggregation is to fit plots of χ vs. t at a series of increasing total protein concentrations. As $[X]_{tot}$ increases, the fit of Eq. 22 to χ vs. t plots should improve (that is, extend to larger and larger portions of the time course) if there is off-pathway aggregation. Fig. 4 illustrates this point. Fig. 4, *A–C*, are plots of synthetic data generated by adding a small, Gaussian-distributed error ($\mu = 0$, $\sigma = 0.02$) to the numerical solutions of the rate equations for the test case described above with $[X]_{tot} = 1$, 10, and 100 μM. The curves in Fig. 4, *A–C*, are fits of Eq. 22 to the data over increasing portions of the time course. For example, the red curve in Fig. 4 *A* is the fit of Eq. 22 to the data up to $\chi = 0.2$, the orange curve to its right is the fit of Eq. 22 to the data up to $\chi = 0.4$, etc. Fig. 4, *A–C*, show that the fit of Eq. 22 to the data improves (in the sense that a good fit to the data is maintained to higher values of χ) as $[X]_{tot}$ increases. This observation is quantified in Fig. 4 *D*, which is a plot of the root mean-square (RMS) residuals of the fits in Fig. 4, *A–C*. At $[X]_{tot} = 1$ μM (i.e., for the data in Fig. 4 *A*), the RMS residuals are roughly constant for fits of Eq. 22 to the data up to $\chi = 0.4$, but they increase thereafter indicating deterioration in the quality of the fit. For $[X]_{tot} = 10$ μM (Fig. 4 *B*), good fits are maintained to $\chi = 0.7$, and for $[X]_{tot} = 100$ μM (Fig. 4 *C*), good fits are maintained essentially until the reaction is complete. The improvement in the fit of Eq. 22 to χ vs. t data as $[X]_{tot}$ increases is a better indication of off-pathway aggregation than the fit itself at a single value of $[X]_{tot}$.

It is usually desirable to use the parameters from fits to experimental data to estimate quantities that are fundamental to a mechanism. Based on Eq. 15 (the more general of the two equations for $[F^{(1)}]$), the relationships of C_1 and C_2 to fundamental quantities are

$$C_1 = \frac{a([F^{(0)}]_0([X_1]_{e,t=0} - K_c) + [X_1]_{e,t=0}^{n+1}(n+1)K_s^{-n+1})}{[F^{(1)}]_{ss}}, \tag{23}$$

and

$$C_2 = \frac{a^2[X_1]_{e,t=0}^{n+1}([X_1]_{e,t=0} - K_c)}{2K_s^{n-1}[F^{(1)}]_{ss}}. \tag{24}$$

Unfortunately, Eqs. 23 and 24 show that C_1 and C_2 are complicated functions of several parameters, one of which ($[X_1]_{e,t=0}$) is itself a complicated function of another parameter (K_A). Unless some parameters are determined independently, it is unlikely that even, for example, determining C_1 and C_2 as functions of concentration would provide reliable estimates of n, K_s, K_A, etc. A better method to estimate parameters is discussed below.

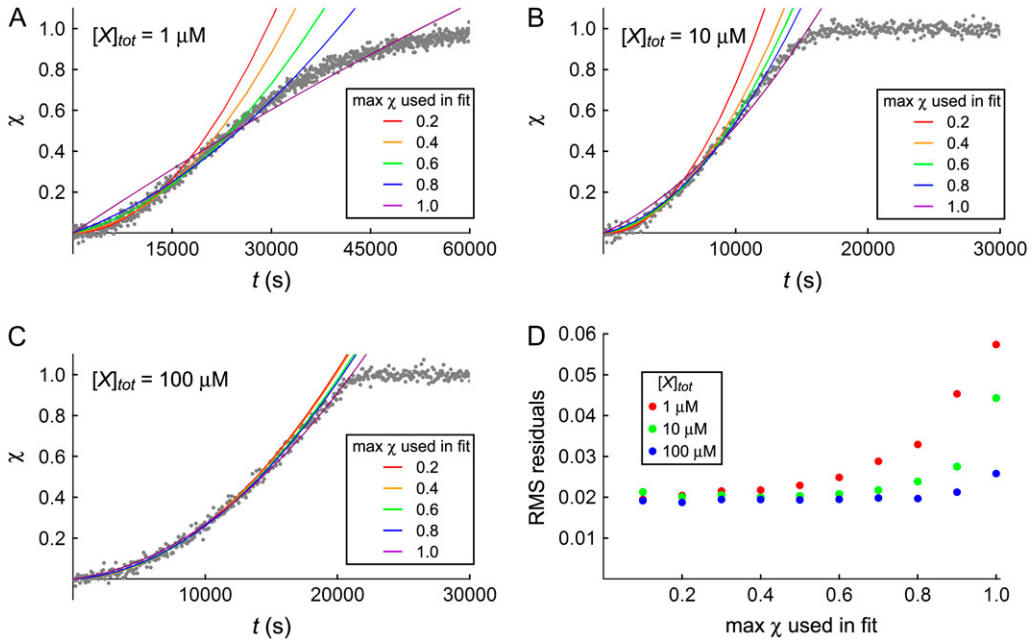

FIGURE 4 (*A–C*) Plots of the extent of completion versus time to simulate fits of Eq. 22 to experimental data at (*A*) $[X]_{tot} = 1$ μM, (*B*) $[X]_{tot} = 10$ μM, and (*C*) $[X]_{tot} = 100$ μM. The gray points are from the numerical solutions to the test case with Gaussian-distributed errors ($\mu = 0$, $\sigma = 0.02$) added to simulate experimental data. The colored curves are fits of Eq. 22 to increasing portions of the data: red, orange, green, blue, and purple curves are fits up to $\chi = 0.2$, 0.4, 0.6, 0.8, and 1.0, respectively. (*D*) A plot of the root mean-square (*RMS*) residuals versus the maximum value of χ used in the fits in *A* (*red circles*), *B* (*green circles*), and *C* (*blue circles*) (note that the RMS residuals are only calculated for the portion of the data that was actually used in the fit).

Connection to experiment: the use of t_{50} vs. $[X]_{tot}$ data

Log-log plots of t_{50} (or similar quantities) versus $[X]_{tot}$ are among the most important tools for studying fibril formation reactions because they conveniently summarize the overall concentration dependence of the rate, and t_{50} values are easily measured (9,20,21,39,40). This feature makes such plots useful for determining the nucleus size in simple nucleated polymerizations: log-log plots of t_{50} vs. $[X]_{tot}$ are linear when $K_c < [X]_{tot} \ll K_s$ with a slope $= -(n + 1)/2$. Curvature in log-log plots of t_{50} vs. $[X]_{tot}$ for a simple nucleated polymerization indicates either that the nucleus size is changing (if n is concentration dependent) (6,45,46) or that $[X]_{tot}$ is approaching K_s (if n is fixed) (9). Log-log plots of t_{50} vs. $[X]_{tot}$ are similarly useful for studying fibril formation reactions that are not simple nucleated polymerizations. Log-log plots of t_{50} vs. $[X]_{tot}$ in which the slope changes from negative to positive or in which the slope is positive throughout are strongly indicative of off-pathway aggregation. In the latter case, when the slope of the plot is always positive, the indication is even stronger if the plot can be fit to the equation

$$t_{50} = \frac{1}{C_3 + \sqrt{C_3^2 + C_4[X]_{tot}^{-1}}}. \quad (25)$$

This equation is based on Eq. 19. (Note that this equation should be valid only when $[X]_{tot} \gg K_A$, in which case $[X_1]_{e,t=0} \sim K_A$, $[F^{(1)}]_{ss} \sim [X]_{tot}$, and $[F^{(0)}]_0([X_1]_{e,t=0} - K_c) \gg ([X_1]_{e,t=0}^{n+1}(n+1))/K_s^{n-1}$. Comparing Eq. 19 to Eqs. 23 and 24 then reveals that $C_3 = C_1$ and $C_4 = [X]_{tot}C_2$.) In the former case, when the plot of t_{50} vs. $[X]_{tot}$ includes the region where the slope changes, inserting Eq. 9 into Eq. 16 yields an equation that can in principle be used to obtain estimates of n and K_A (a and K_s cannot be determined independently). However, the equation is complicated and the parameter estimates obtained by using it are only moderately accurate. Better (though not perfect) estimates of n can be obtained by two methods if the initial monomer concentration in equilibrium with off-pathway aggregates ($[X_1]_{e,t=0}$) can be measured independently by using, for example, gel filtration early in the fibril formation time course. In the first method, the approximation $([X_1]_{e,t=0} - K_c) \sim [X_1]_{e,t=0}$ is made and Eq. 16 is rewritten as follows

$$\log_{10} t_{50} - \frac{\log_{10}[X]_{tot}}{2} = C_5 - \frac{n+2}{2}\log_{10}[X_1]_{e,t=0}, \quad (26)$$

where C_5 is a constant equal to $0.5\ (n - 1)\ \log_{10} K_s/a$. The value of n can then be estimated from the slope of a plot of $\log_{10} t_{50} - 0.5 \log_{10} [X]_{tot}$ vs. $\log_{10} [X_1]_{e,t=0}$. Alternately, the value of K_A can be estimated by measuring $[X_1]_{e,t=0}$ at a series of total protein concentrations and fitting Eq. 9 to a plot of $[X_1]_{e,t=0}$ vs. $[X]_{tot}$. Given such an estimate of K_A and the value of $[X]_{tot}$ at which t_{50} is a minimum, n can be estimated using Eq. 17.

Connection to experiment: the use of light scattering data

The total intensity of scattered light from protein solutions undergoing a nucleated polymerization with off-pathway aggregation is the sum of the intensities of the light scattered by off-pathway aggregates and fibrils. Light scattering by particles in solution depends on a number of factors, the most important for our purposes being the particle shape and size relative to the wavelength of incident light (λ), or rather, particle size relative to the quantity $\lambda/[2\pi \sin(\theta/2)]$, where θ is the angle of detection (for the sake of argument in the paragraphs that follow, we take $\lambda = 500$ nm and $\theta = 90°$ so that $\lambda/[2\pi \sin(\theta/2)] \sim 110$ nm).

Off-pathway aggregates are likely to be small relative to $\lambda/[2\pi \sin(\theta/2)]$ for two reasons. First, off-pathway aggregates are expected to be roughly spherical, so their linear dimensions (i.e., their diameters, D) should scale with the cube root of their masses, and therefore with the cube root of the number of subunits in the aggregates; that is, for Z_j, $D \propto j^{1/3}$. Second, the size-average size of the off-pathway aggregates ($\langle j \rangle_{w,agg}$) is

$$\langle j \rangle_{w,agg} = \frac{\sum_{j=1}^{\infty} j^2[Z_j]}{\sum_{j=1}^{\infty} j[Z_j]} = \frac{\sum_{j=1}^{\infty} j^2[X_1]_e^j/K_A^{j-1}}{[A]} = \frac{[A]\sqrt{4[A]K_A^{-1}+1}}{[A]}$$
$$= \sqrt{4[A]K_A^{-1}+1}. \quad (27)$$

(We use the phrase ''size-average size'' here to mean the weight-average molecular weight divided by the molar mass of a monomer.) The value of $[A]$, and therefore $\langle j \rangle_{w,agg}$, is largest at the beginning of the fibril formation reaction, when $[A] = [X]_{tot}$. The maximum value of $\langle j \rangle_{w,agg}$ is therefore proportional to the square root of $[X]_{tot}/K_A$. Combining these two points reveals that the average diameter of off-pathway aggregates should only increase as the sixth root of $[X]_{tot}/K_A$. Globular proteins typically have densities around 1.4 g/cm^3 (47); assuming that off-pathway aggregates are packed at least 10% as efficiently as globular proteins (density ~0.14 g/cm^3) and that the molar mass of a monomer is ~10 kDa, a rough calculation indicates that $[X]_{tot}/K_A$ would have to be on the order of 1000 for the average off-pathway aggregate to have $D \sim 25$ nm, or ~20% of $\lambda/[2\pi \sin(\theta/2)]$.

Because off-pathway aggregates are small relative to $\lambda/[2\pi \sin(\theta/2)]$, the intensity of light scattered by them ($i_{s,agg}$) depends on the second moment of their size distribution (48):

$$i_{s,agg} = Q\sum_{j=1}^{\infty} j^2[Z_j] = Q\left([A]\sqrt{4[A]K_A^{-1}+1}\right), \quad (28)$$

where Q is a constant that depends on the index of refraction of the solution, the refractive index increment of the protein, the wavelength and intensity of incident light, the distance from the sample to the detector, and the angle of detection. If

$4[A]K_A^{-1} \gg 1$, as it is in the test case for much of the fibril formation time course if $[X]_{tot}$ is large enough ($[X]_{tot} > 10$ μM), this simplifies to

$$i_{s,agg} = 2QK_A^{-1/2}[A]^{3/2}. \quad (29)$$

In contrast to off-pathway aggregates, fibrils are expected to have linear dimensions (i.e., lengths, L) that become larger than $\lambda/[2\pi \sin(\theta/2)]$ early in the fibril formation time course. It can be shown (see Supplementary Material) that the intensity of light scattered by fibrils ($i_{s,fib}$) in this size range (assuming they can be treated as thin, stiff rods) should be directly proportional to $[F^{(1)}]$, the first moment of fibril size distribution (49):

$$i_{s,fib} = \frac{Q\sum_{j=1}^{\infty} j[Y_j]}{4l\lambda^{-1}\sin(\theta/2)} = \frac{Q[F^{(1)}]}{4l\lambda^{-1}\sin(\theta/2)}, \quad (30)$$

where l is the length increment per subunit for fibrils. To support our statement that fibril lengths can rapidly become larger than $\lambda/[2\pi\sin(\theta/2)]$, we show in the Supplementary Material that the size average size of fibrils increases with time roughly as follows:

$$\langle j\rangle_{w,fib} = \frac{\sum_{j=1}^{\infty} j^2[Y_j]}{\sum_{j=1}^{\infty} j[Y_j]} \cong \frac{2a([X_1]_{e,t=0} - K_c)t}{3}. \quad (31)$$

For the test case, with $a = 10^6\ M^{-1}\ s^{-1}$ and $K_c = 100$ nM, the right-hand side of Eq. 31 is $\sim 0.2t$ at $[X]_{tot} = 1$ μM ($[X_1]_{e,t=0} = 380$ nM). We assume that a fibrillogenic protein with a molar mass of 10 kDa will form fibrils that extend by $\sim$1 nm for every two subunits added, giving a mass-per-length that is roughly typical of amyloid fibrils (20 kDa/nm) (50–53). According to Eq. 31, the average fibril length for such a protein will be 200 nm ($\langle j\rangle_{w,fib} = 400$) after $\sim$2000 s at $[X]_{tot} = 1$ μM. This rough calculation indicates that the fibrils formed in the test case will be substantially larger than $\lambda/[2\pi \sin(\theta/2)]$ well before t_{50} is reached ($\lambda/[2\pi \sin(\theta/2)]$ is exceeded even faster at higher protein concentrations).

Given the assumptions and approximations made above, the total intensity of light scattered by a mixture of off-pathway aggregates and fibrils ($i_{s,tot}$) should be

$$i_{s,tot} = i_{s,agg} + i_{s,fib} = 2QK_A^{-1/2}[A]^{3/2} + \frac{Q[F^{(1)}]}{4l\lambda^{-1}\sin(\theta/2)}, \quad (32)$$

where l is $\sim$0.5 nm in our example. Noting that $[F^{(1)}] = \chi[F^{(1)}]_{ss}$ and $[A] = [X]_{tot} - [F^{(1)}] = [X]_{tot} - \chi[F^{(1)}]_{ss}$ and using Eq. 22 for χ reveals that the time dependence of $i_{s,tot}$ has the form:

$$i_{s,tot} = (Q_1 - Q_2 t - Q_3 t^2)^{3/2} + Q_4 t + Q_5 t^2, \quad (33)$$

where $Q_1 = (2QK_A^{-1/2})^{2/3}[X]_{tot}$, $Q_2 = (2QK_A^{-1/2})^{2/3}\,[F^{(1)}]_{ss}C_1$, $Q_3 = (2QK_A^{-1/2})^{2/3}[F^{(1)}]_{ss}C_2$, $Q_4 = (Q[F^{(1)}]_{ss}C_1)/(4l\lambda^{-1}\sin(\theta/2))$, and $Q_5 = (Q[F^{(1)}]_{ss}C_2)/(4l\lambda^{-1}\sin(\theta/2))$, and C_1 and C_2 are the same constants used in Eq. 22. If a protein forms fibrils by a nucleated polymerization with an off-pathway aggregation, it should be possible to fit Eq. 33 to a plot of scattered light intensity versus time, but all of the limitations of Eq. 22 apply to Eq. 33. Thus, Eq. 33 should fit to only the initial part of the scattered light intensity time course at low $[X]_{tot}$, but the fit should improve (i.e., fit to larger and larger portions of the time course) as $[X]_{tot}$ increases. Also, it is worth noting that only four of the five parameters in Eq. 33 are independent, because $Q_2/Q_3 = Q_4/Q_5 = C_1/C_2$. It could be helpful when fitting Eq. 33 to data to replace Q_4 with Q_2Q_5/Q_3, thereby reducing by one the dimensionality of the search for best-fit parameters.

DISCUSSION

Identifying a nucleated polymerization with an off-pathway aggregation

Whether nonfibrillar aggregates appear during a fibril formation reaction can be determined directly by using atomic force or electron microscopy. These techniques, however, are not as useful for determining the role of these aggregates in a fibril formation mechanism as they are for establishing their existence. In the Results section, we presented three tests that can be applied to experimental data to identify off-pathway aggregates. These are: 1), Fitting Eq. 22 to χ vs. t data obtained at a series of total protein concentrations. An improving fit as $[X]_{tot}$ increases is an indication that the aggregates are off-pathway. (Note that a good fit throughout the time course that remained good as $[X]_{tot}$ increased would also be an indication of off-pathway aggregation). 2), Making a log-log plot of t_{50} vs. $[X]_{tot}$. A change in slope from negative to positive, or a positive slope throughout that can be fit by Eq. 25 indicates that the aggregates are off-pathway. The plot can also be used to estimate n and K_A, especially if $[X_1]_{e,t=0}$ can be measured independently (see above). 3), Fitting Eq. 33 to light scattering intensity versus t data. In this test, a good fit of the equation to the data is itself an indication that the aggregates are off-pathway, which becomes stronger if the fit improves as $[X]_{tot}$ increases.

It is difficult to categorize positive results in the tests listed above as necessary and/or sufficient for identifying off-pathway aggregation because the effects of other types of aggregates (on-pathway or obligate) on the relevant experimental observables have not been determined to our knowledge. A positive result in the first test is certainly necessary, but may not be sufficient. A positive result in the second test may be sufficient, but because high values of $[X]_{tot}$ may be required to observe the sign change in the slope of a log-log plot of t_{50} vs. $[X]_{tot}$, it is not necessary. Similarly, a positive result in the third test may be sufficient but cannot be considered necessary. Several approximations about how

fibrils and off-pathway aggregates scatter light were used to derive Eq. 33; a conspiracy of unfortunate conditions could result in these approximations becoming invalid even if the mechanism were in fact a nucleated polymerization with off-pathway aggregation. (For example, fibrils are perhaps better approximated as semiflexible chains (54,55) than thin, stiff rods. Also, at high concentrations, interactions between fibrils could ruin the proportionality between light scattering and $[F^{(1)}]$.) These tests are likely to be useful in different situations. For example, time-dependent light scattering intensities are best measured with a light scattering photometer (although they can be measured with an ordinary fluorometer (56)). Acquiring this type of data therefore has more intensive instrumentation requirements than measuring χ vs. t by dye binding. Hence, the first two tests are more accessible than the third. On the other hand, if off-pathway aggregates interfere with the dye binding assays used to measure χ vs. t (for example, we have observed binding to amorphous aggregates to induce thioflavin T fluorescence (12,39,40,57)) then the third test may be the only option. Finally, if concentrations high enough to cause the log-log plot of t_{50} vs. $[X]_{tot}$ to change slope cannot be reached practically, the first and third tests would be more useful than the second. We currently believe that a robust identification of off-pathway aggregation should ideally involve direct observation of nonfibrillar aggregates that eventually disappear in favor of fibrils and positive results with two of the above three tests.

Off-pathway aggregates versus off-pathway micelles

Nonfibrillar aggregates formed by proteins are often categorized as micelles (18,19,34,58–60). Micelles differ from the downhill-type aggregates in our model in that they have a preferred size (61,62). This preferred size is usually large enough for micelle formation to behave like a phase transition: micelles do not form when the protein concentration is below a certain concentration, called the critical micelle concentration (61,62). Above the critical micelle concentration, the monomer concentration is roughly constant and excess protein forms micelles. Off-pathway micelles should therefore buffer the monomer concentration just as off-pathway aggregates do, and fibril formation by proteins that form off-pathway micelles should have characteristics similar to those of fibril formation by proteins that form off-pathway aggregates. These characteristics should include a quadratic dependence of χ on t when the total protein concentration is substantially higher than the critical micelle concentration, and log-log plots of t_{50} vs. $[X]_{tot}$ in which the slope changes from negative to positive at some concentration. There is, however, one caveat: the behavior described above would not be observed if the off-pathway micelles formed by a protein were small (e.g., dimers, trimers, etc.), because then ''micelle'' formation would have the properties of a finite oligomerization rather than a phase transition (monomer-dimer, monomer-trimer, etc. equilibria do not have critical concentrations). Compared to mechanisms with monomer-off-pathway aggregate or monomer-micelle equilibria, the monomer concentration would change rapidly as protein was consumed by fibril formation in a mechanism with a monomer-off-pathway small oligomer equilibrium, especially at high total protein concentration. Monomer-small oligomer equilibria cannot buffer the monomer concentration as effectively as monomer-aggregate or monomer-micelle equilibria can.

Implications of off-pathway aggregation

Off-pathway aggregation substantially slows fibril formation reactions. In the test case examined above, using the parameters listed in the Results section and $[X]_{tot} = 10$ μM, the t_{50} for fibril formation was 93,000 s, or ~25 h. A simple nucleated polymerization with the same parameters would be three orders of magnitude faster, with a t_{50} of ~80 s (data not shown). Furthermore, the t_{50} of 93,000 s quoted above was obtained with a, the monomer-fibril association rate constant, set to 10^6 M^{-1} s^{-1}, which is a typical protein-protein association rate constant (31,63). However, association rate constants two and three orders of magnitude smaller have also been reported (64). Changing a to 10^4 M^{-1} s^{-1} and adjusting the other kinetic parameters so that K_c, K_s, and K_A remain constant (i.e., setting $c = 10^{-3}$ s^{-1}, $b = 1$ s^{-1}, $\alpha = 10^5$ M^{-1} s^{-1}, and $\beta = 10^{-1}$ s^{-1}) would give a t_{50} of ~110 days. On-pathway and obligate aggregates are not expected to slow fibril formation in this way, or to persist for nearly as long as off-pathway aggregates.

We expect that nucleated polymerization with off-pathway aggregation will be found to be a rare fibril formation mechanism, as off-pathway aggregates ought to be able to rearrange into on-pathway oligomers or fibrils. However, for proteins that are found to aggregate by a mechanism that approaches nucleated polymerization with off-pathway aggregation (because rearrangement is either slow or nonexistent), the potentially long lifetimes of the aggregates could have important implications for protein aggregation diseases. Nonfibrillar protein aggregates have been found in many contexts to be more toxic than fibrils (65–70). Proteins that form aggregates that convert slowly and indirectly into fibrils would therefore be expected to be more harmful than those that form aggregates that convert rapidly and directly, or those that form fibrils without nonfibrillar intermediates. Off-pathway aggregates are more dangerous than on-pathway or obligate aggregates in this sense. Worse, off-pathway aggregates can become even longer lived as the protein concentration increases. Off-pathway aggregates can thus be doubly detrimental: their lifetimes can increase as they become more abundant. These features of off-pathway aggregates give nucleated polymerization with an off-pathway aggregation the potential to be a particularly malign fibril formation mechanism.

SUPPLEMENTARY MATERIAL

To view all of the supplemental files associated with this article, visit www.biophysj.org.

This work was supported by the National Institutes of Health (grant No. NS050636).

REFERENCES

1. Selkoe, D. J. 2003. Folding proteins in fatal ways. *Nature*. 426:900–904.
2. Pepys, M. B. 2006. Amyloidosis. *Annu. Rev. Med.* 57:223–241.
3. Hardy, J., and D. J. Selkoe. 2002. Medicine—the amyloid hypothesis of Alzheimer's disease: progress and problems on the road to therapeutics. *Science*. 297:353–356.
4. Fink, A. L. 2006. The aggregation and fibrillation of alpha-synuclein. *Acc. Chem. Res.* 39:628–634.
5. Buxbaum, J. N. 2003. Diseases of protein conformation: what do in vitro experiments tell us about in vivo diseases? *Trends Biochem. Sci.* 28:585–592.
6. Ferrone, F. A. 2006. Nucleation: the connections between equilibrium and kinetic behavior. *Methods Enzymol.* 412:285–299.
7. Oosawa, F., and S. Asakura. 1975. Thermodynamics of the Polymerization of Protein. Academic Press, London, UK.
8. Andrews, J. M., and C. J. Roberts. 2007. A Lumry-Eyring nucleated polymerization model of protein aggregation kinetics. 1. Aggregation with pre-equilibrated unfolding. *J. Phys. Chem. B*. 111:7897–7913.
9. Powers, E. T., and D. L. Powers. 2006. The kinetics of nucleated polymerizations at high concentrations: amyloid fibril formation near and above the ''supercritical concentration''. *Biophys. J.* 91:122–132.
10. Ahmad, A., V. N. Uversky, D. Hong, and A. L. Fink. 2005. Early events in the fibrillation of monomeric insulin. *J. Biol. Chem.* 280: 42669–42675.
11. Baskakov, I. V., G. Legname, M. A. Baldwin, S. B. Prusiner, and F. E. Cohen. 2002. Pathway complexity of prion protein assembly into amyloid. *J. Biol. Chem.* 277:21140–21148.
12. Bieschke, J., Q. H. Zhang, E. T. Powers, R. A. Lerner, and J. W. Kelly. 2005. Oxidative metabolites accelerate Alzheimer's amyloidogenesis by a two-step mechanism, eliminating the requirement for nucleation. *Biochemistry*. 44:4977–4983.
13. Bitan, G., A. Lomakin, and D. B. Teplow. 2001. Amyloid beta-protein oligomerization: prenucleation interactions revealed by photo-induced cross-linking of unmodified proteins. *J. Biol. Chem.* 276:35176–35184.
14. Conway, K. A., S. J. Lee, J. C. Rochet, T. T. Ding, R. E. Williamson, and P. T. Lansbury. 2000. Acceleration of oligomerization, not fibrillization, is a shared property of both alpha-synuclein mutations linked to early-onset Parkinson's disease: implications for pathogenesis and therapy. *Proc. Natl. Acad. Sci. USA*. 97:571–576.
15. Kaylor, J., N. Bodner, S. Edridge, G. Yamin, D. P. Hong, and A. L. Fink. 2005. Characterization of oligomeric intermediates in alpha-synuclein fibrillation: FRET studies of Y125W/Y133F/Y136F alpha-synuclein. *J. Mol. Biol.* 353:357–372.
16. Kirkitadze, M. D., M. M. Condron, and D. B. Teplow. 2001. Identification and characterization of key kinetic intermediates in amyloid beta-protein fibrillogenesis. *J. Mol. Biol.* 312:1103–1119.
17. Plakoutsi, G., F. Bemporad, M. Calamai, N. Taddei, C. M. Dobson, and F. Chiti. 2005. Evidence for a mechanism of amyloid formation involving molecular reorganisation within native-like precursor aggregates. *J. Mol. Biol.* 351:910–922.
18. Rhoades, E., J. Agarwal, and A. Gafni. 2000. Aggregation of an amyloidogenic fragment of human islet amyloid polypeptide. *Biochim. Biophys. Acta*. 1476:230–238.
19. Sabate, R., and J. Estelrich. 2005. Evidence of the existence of micelles in the fibrillogenesis of beta-amyloid peptide. *J. Phys. Chem. B*. 109: 11027–11032.
20. Serio, T. R., A. G. Cashikar, A. S. Kowal, G. J. Sawicki, J. J. Moslehi, L. Serpell, M. F. Arnsdorf, and S. L. Lindquist. 2000. Nucleated conformational conversion and the replication of conformational information by a prion determinant. *Science*. 289:1317–1321.
21. Sokolowski, F., A. J. Modler, R. Masuch, D. Zirwer, M. Baier, G. Lutsch, D. A. Moss, K. Gast, and D. Naumann. 2003. Formation of critical oligomers is a key event during conformational transition of recombinant Syrian hamster prion protein. *J. Biol. Chem.* 278:40481–40492.
22. Souillac, P. O., V. N. Uversky, I. S. Millett, R. Khurana, S. Doniach, and A. L. Fink. 2002. Elucidation of the molecular mechanism during the early events in immunoglobulin light chain amyloid fibrillation. Evidence for an off-pathway oligomer at acidic pH. *J. Biol. Chem.* 277:12666–12679.
23. Souillac, P. O., V. N. Uversky, and A. L. Fink. 2003. Structural transformations of oligomeric intermediates in the fibrillation of the immunoglobulin light chain LEN. *Biochemistry*. 42:8094–8104.
24. Teplow, D. B., N. D. Lazo, G. Bitan, S. Bernstein, T. Wyttenbach, M. T. Bowers, A. Baumketner, J. E. Shea, B. Urbanc, L. Cruz, J. Borreguero, and H. E. Stanley. 2006. Elucidating amyloid beta-protein folding and assembly: a multidisciplinary approach. *Acc. Chem. Res.* 39:635–645.
25. Ferrone, F. 1999. Analysis of protein aggregation kinetics. *Methods Enzymol.* 309:256–274.
26. Goldstein, R. F., and L. Stryer. 1986. Cooperative polymerization reactions: analytical approximations, numerical examples, and experimental strategy. *Biophys. J.* 50:583–599.
27. Hill, T. L. 1987. Linear Aggregation Theory in Cell Biology. Springer-Verlag, Berlin, Germany.
28. Roberts, C. J. 2003. Kinetics of irreversible protein aggregation: analysis of extended Lumry-Eyring models and implications for predicting protein shelf life. *J. Phys. Chem. B*. 107:1194–1207.
29. McCoy, B. J. 2001. Distribution kinetics modeling of nucleation, growth, and aggregation processes. *Ind. Eng. Chem. Res.* 40:5147–5154.
30. Janin, J. 1997. The kinetics of protein-protein recognition. *Proteins*. 28:153–161.
31. Northrup, S. H., and H. P. Erickson. 1992. Kinetics of protein-protein association explained by Brownian dynamics computer simulation. *Proc. Natl. Acad. Sci. USA*. 89:3338–3342.
32. Schlosshauer, M., and D. Baker. 2002. A general expression for bimolecular association rates with orientational constraints. *J. Phys. Chem. B*. 106:12079–12083.
33. Firestone, M. P., R. Delevie, and S. K. Rangarajan. 1983. On one dimensional nucleation and growth of living polymers. 1. Homogeneous nucleation. *J. Theor. Biol.* 104:535–552.
34. Rhoades, E., and A. Gafni. 2003. Micelle formation by a fragment of human islet amyloid polypeptide. *Biophys. J.* 84:3480–3487.
35. Kunes, K. C., D. L. Cox, and R. R. P. Singh. 2005. One-dimensional model of yeast prion aggregation. *Phys. Rev. E*. 72:051915.
36. Powers, E. T., and D. L. Powers. 2003. A perspective on mechanisms of protein tetramer formation. *Biophys. J.* 85:3587–3599.
37. LeVine, H. 1999. Quantification of beta-sheet amyloid fibril structures with thioflavin T. *Methods Enzymol.* 309:274–284.
38. Nilsson, M. R. 2004. Techniques to study amyloid fibril formation in vitro. *Methods*. 34:151–160.
39. Frankenfield, K. N., E. T. Powers, and J. W. Kelly. 2005. Influence of the N-terminal domain on the aggregation properties of the prion protein. *Protein Sci.* 14:2154–2166.
40. Hurshman, A. R., J. T. White, E. T. Powers, and J. W. Kelly. 2004. Transthyretin aggregation under partially denaturing conditions is a downhill polymerization. *Biochemistry*. 43:7365–7381.
41. O'Nuallain, B., A. K. Thakur, A. D. Williams, A. M. Bhattacharyya, S. Chen, G. Thiagarajan, and R. Wetzel. 2006. Kinetics and thermodynamics of amyloid assembly using a high-performance liquid chromatography-based sedimentation assay. *Methods Enzymol.* 413:34–74.

42. Mok, Y. F., and G. J. Howlett. 2006. Sedimentation velocity analysis of amyloid oligomers and fibrils. *Methods Enzymol.* 413:199–217.

43. Rogers, S. S., P. Venema, L. M. C. Sagis, E. van der Linden, and A. M. Donald. 2005. Measuring the length distribution of a fibril system: a flow birefringence technique applied to amyloid fibrils. *Macromolecules.* 38:2948–2958.

44. Chen, S., F. A. Ferrone, and R. Wetzel. 2002. Huntington's disease age-of-onset linked to polyglutamine aggregation nucleation. *Proc. Natl. Acad. Sci. USA.* 99:11884–11889.

45. Ferrone, F. A., J. Hofrichter, and W. A. Eaton. 1985. Kinetics of sickle hemoglobin polymerization. 1. Studies using temperature-jump and laser photolysis techniques. *J. Mol. Biol.* 183:591–610.

46. Ferrone, F. A., J. Hofrichter, and W. A. Eaton. 1985. Kinetics of sickle hemoglobin polymerization. 2. A double nucleation mechanism. *J. Mol. Biol.* 183:611–631.

47. Chalikian, T. V., M. Totrov, R. Abagyan, and K. J. Breslauer. 1996. The hydration of globular proteins as derived from volume and compressibility measurements: cross correlating thermodynamic and structural data. *J. Mol. Biol.* 260:588–603.

48. Oster, G. 1947. Light scattering from polymerizing and coagulating systems. *J. Colloid Sci.* 2:291–299.

49. Berne, B. J. 1974. Interpretation of the light scattering from long rods. *J. Mol. Biol.* 89:755–758.

50. Bauer, H. H., U. Aebi, M. Haner, R. Hermann, M. Muller, and H. P. Merkle. 1995. Architecture and polymorphism of fibrillar supramolecular assemblies produced by in vitro aggregation of human calcitonin. *J. Struct. Biol.* 115:1–15.

51. Cardoso, I., C. S. Goldsbury, S. A. Muller, V. Olivieri, S. Wirtz, A. M. Damas, U. Aebi, and M. J. Saraiva. 2002. Transthyretin fibrillogenesis entails the assembly of monomers: a molecular model for in vitro assembled transthyretin amyloid-like fibrils. *J. Mol. Biol.* 317:683–695.

52. Goldsbury, C. S., G. J. Cooper, K. N. Goldie, S. A. Muller, E. L. Saafi, W. T. Gruijters, M. P. Misur, A. Engel, U. Aebi, and J. Kistler. 1997. Polymorphic fibrillar assembly of human amylin. *J. Struct. Biol.* 119: 17–27.

53. Goldsbury, C. S., S. Wirtz, S. A. Muller, S. Sunderji, P. Wicki, U. Aebi, and P. Frey. 2000. Studies on the in vitro assembly of Abeta 1–40: implications for the search for a beta fibril formation inhibitors. *J. Struct. Biol.* 130:217–231.

54. Pallitto, M. M., and R. M. Murphy. 2001. A mathematical model of the kinetics of beta-amyloid fibril growth from the denatured state. *Biophys. J.* 81:1805–1822.

55. Shen, C. L., M. C. Fitzgerald, and R. M. Murphy. 1994. Effect of acid predissolution on fibril size and fibril flexibility of synthetic beta-amyloid peptide. *Biophys. J.* 67:1238–1246.

56. Chen, S., V. Berthelier, J. B. Hamilton, B. O'Nuallain, and R. Wetzel. 2002. Amyloid-like features of polyglutamine aggregates and their assembly kinetics. *Biochemistry.* 41:7391–7399.

57. Zhang, Q. H., E. T. Powers, J. Nieva, M. E. Huff, M. A. Dendle, J. Bieschke, C. G. Glabe, A. Eschenmoser, P. Wentworth, R. A. Lerner, and J. W. Kelly. 2004. Metabolite-initiated protein misfolding may trigger Alzheimer's disease. *Proc. Natl. Acad. Sci. USA.* 101:4752–4757.

58. Yong, W., A. Lomakin, M. D. Kirkitadze, D. B. Teplow, S. H. Chen, and G. B. Benedek. 2002. Structure determination of micelle-like intermediates in amyloid beta-protein fibril assembly by using small angle neutron scattering. *Proc. Natl. Acad. Sci. USA.* 99:150–154.

59. Lomakin, A., D. B. Teplow, D. A. Kirschner, and G. B. Benedek. 1997. Kinetic theory of fibrillogenesis of amyloid beta-protein. *Proc. Natl. Acad. Sci. USA.* 94:7942–7947.

60. Lomakin, A., D. S. Chung, G. B. Benedek, D. A. Kirschner, and D. B. Teplow. 1996. On the nucleation and growth of amyloid beta-protein fibrils: detection of nuclei and quantitation of rate constants. *Proc. Natl. Acad. Sci. USA.* 93:1125–1129.

61. Puvvada, S., and D. Blankschtein. 1990. Molecular-thermodynamic approach to predict micellization, phase behavior and phase separation of micellar solutions. 1. Application to nonionic surfactants. *J. Chem. Phys.* 92:3710–3724.

62. Tanford, C. 1980. The Hydrophobic Effect: Formation of Micelles and Biological Membranes. John Wiley & Sons, New York.

63. Schreiber, G. 2002. Kinetic studies of protein-protein interactions. *Curr. Opin. Struct. Biol.* 12:41–47.

64. Koren, R., and G. G. Hammes. 1976. A kinetic study of protein-protein interactions. *Biochemistry.* 15:1165–1171.

65. Bucciantini, M., E. Giannoni, F. Chiti, F. Baroni, L. Formigli, J. Zurdo, N. Taddei, G. Ramponi, C. M. Dobson, and M. Stefani. 2002. Inherent toxicity of aggregates implies a common mechanism for protein misfolding diseases. *Nature.* 416:507–511.

66. Haass, C., and D. J. Selkoe. 2007. Soluble protein oligomers in neurodegeneration: lessons from the Alzheimer's amyloid beta-peptide. *Nat. Rev. Mol. Cell Biol.* 8:101–112.

67. Klein, W. L., W. B. Stine Jr., and D. B. Teplow. 2004. Small assemblies of unmodified amyloid beta-protein are the proximate neurotoxin in Alzheimer's disease. *Neurobiol. Aging.* 25:569–580.

68. Lambert, M. P., A. K. Barlow, B. A. Chromy, C. Edwards, R. Freed, M. Liosatos, T. E. Morgan, I. Rozovsky, B. Trommer, K. L. Viola, P. Wals, C. Zhang, et al. 1998. Diffusible, nonfibrillar ligands derived from Abeta1-42 are potent central nervous system neurotoxins. *Proc. Natl. Acad. Sci. USA.* 95:6448–6453.

69. Reixach, N., S. Deechongkit, X. Jiang, J. W. Kelly, and J. N. Buxbaum. 2004. Tissue damage in the amyloidoses: transthyretin monomers and nonnative oligomers are the major cytotoxic species in tissue culture. *Proc. Natl. Acad. Sci. USA.* 101:2817–2822.

70. Silveira, J. R., G. J. Raymond, A. G. Hughson, R. E. Race, V. L. Sim, S. F. Hayes, and B. Caughey. 2005. The most infectious prion protein particles. *Nature.* 437:257–261.